

Magnification Probability Distribution Functions of Standard Candles in a Clumpy Universe

Chul-Moon YOO,^{1,2,3} Hideki ISHIHARA,² Ken-ichi NAKAO²
and Hideyuki TAGOSHI⁴

¹*Yukawa Institute for Theoretical Physics,
Kyoto University Kyoto 606-8502, Japan*

²*Department of Physics, Graduate School of Science,
Osaka City University Osaka 558-8585, Japan*

³*Asia Pacific Center for Theoretical Physics,
Pohang University of Science and Technology, Pohang 790-784, Korea*

⁴*Department of Earth and Space Science, Graduate School of Science,
Osaka University, Toyonaka 560-0043, Japan*

Abstract

Lensing effects on light rays from point light sources, such like Type Ia supernovae, are simulated in a clumpy universe model. In our universe model, it is assumed that all matter in the universe takes the form of randomly distributed objects each of which has finite size and is transparent for light rays. Monte-Carlo simulations are performed for several lens models, and we compute probability distribution functions of magnification. In the case of the lens models that have a smooth density profile or the same degree of density concentration as the spherical NFW (Navarro-Frenk-White) lens model at the center, the so-called gamma distributions fit well the magnification probability distribution functions if the size of lenses is sufficiently larger than the Einstein radius. In contrast, the gamma distributions do not fit the magnification probability distribution functions in the case of the SIS (Singular Isothermal Sphere) lens model. We find, by using the power law cusp model, that the magnification probability distribution function is fitted well using the gamma distribution only when the slope of the central density profile is not very steep. These results suggest that we may obtain information about the slope of the central density profiles of dark matter halo from the lensing effect of Type Ia supernovae.

§1. Introduction

Type Ia supernovae (SNe) are very useful tools to investigate our universe. For example, the distance-redshift relation obtained as a result of the observations of these strongly suggests the present acceleration of the cosmic volume expansion of our universe.^{1)–4)} To confirm this indication, further projects, such as the ESSENCE project at NOAO,^{*)} the Large Synoptic Survey Telescope^{**)} and Supernova/Acceleration Probe (SNAP),^{***)} are now active or planned.

Current observational data points on the distance-redshift plane are somewhat scattered, and this is an origin of the error in estimating the cosmological parameters. One of the reasons for this distance dispersion is gravitational lensing effects due to the mass inhomogeneities in our universe. Although the dispersion due to gravitational lensing is relatively smaller than other effects at low redshift, it may become more prominent and comparable to the intrinsic dispersion at high redshift $z \gtrsim 1.2$.^{5),6)} In this sense, the mass inhomogeneities are obstacles to the determination of the cosmological parameters through the observation of Type Ia SNe. On the other hand, the mass inhomogeneities contain rich information about the physical process of the evolution of our universe. Thus, the mass inhomogeneities themselves are very significant subjects in cosmology.

We can understand the property of the mass inhomogeneities by comparing the observational data about type Ia SNe with theoretical predictions obtained through the investigations of the gravitational lensing effects on the light rays from them. This is just the purpose of this paper.

There are many works about gravitational lensing related to SNe: effects on SNe observations,^{6)–15)} their availability for investigation of our universe,^{16)–22)} the extraction of the evidence for lensing effects from observational data^{23)–26)} and others.^{27),28),30)–36)}

In this paper, we particularly focus on the effects of small-scale structures. The smaller scale inhomogeneity may affect the apparent magnitude of sources owing to gravitational focusing. The mass scale of the inhomogeneities, which is considered in this paper, is between $10^{-2}M_{\odot}$ and $10^{10}M_{\odot}$. There are several works related to this subject.^{16)–18),27),28)} In these works, compact lens objects were mainly studied, whereas, in this paper, we consider the extended lens objects. Even in the case of the extended lens objects, the strong lensing effects that cause multiple images are of considerable importance if the density profiles of the objects are significantly steep at the center.

*) <http://www.ctio.noao.edu/wproject/>

***) http://www.lsst.org/lsst_home.shtml

***) <http://snap.lbl.gov>

We consider the flat Λ CDM model with $\Omega_{A0} = 0.71$, $\Omega_{m0} = 0.29$ as the starting point. In the cold dark matter cosmology, the first objects to form are of subgalactic size. Then, larger structures form through tidal interaction and mergers of smaller objects. Therefore, the dark matter may form numerous clumps. For simplicity, we assume that all matter in the universe takes the form of randomly distributed objects, each of which has finite size and is transparent for light rays. We investigate the magnification effect due to the gravitational lensing on light rays from the point sources such as Type Ia supernovae. The light rays from distant supernova events suffer multiple gravitational lensing effects from the clumps in the universe. The propagation of the light rays is thus stochastic owing to the randomness of the distribution of the clumps. In this paper, we focus on magnification probability distribution function (MPDF). We introduce a simple method to simulate multiple gravitational lensing effects in the clumpy universe model, which is based on our previous study.³⁸⁾ We perform Monte-Carlo simulations for several lens models, and we investigate the dependence of the MPDF on lens models of dark matter clumps.

Throughout this paper, it is assumed that light sources are pointwise. This assumption is valid only when the linear extent of a source is much smaller than the Einstein radius of each lens object. The linear extent of the SNe is of the order of $\sim 10^{15}$ cm, which is the typical radius of SNe at the peak brightness. The Einstein radius of a lens object of mass M_L is of the order $\sqrt{GM_L D/c^2}$, where D is the distance to supernovae, G and c are the gravitational constant and speed of light, respectively. Therefore, we assume that M_L satisfies $\sqrt{GM_L D/c^2} \gg 10^{15}$ cm. Because in the case of high-redshift supernova events, $D \sim 1$ Gpc, this assumption leads

$$M_L \gg 10^{-2} M_{\odot}. \quad (1.1)$$

Our method is complementary to the methods using the N-body simulation. In the N-body simulation, the nonlinear time evolution and the spatial correlation of the dark matter distribution can be studied. Very large scale N-body simulations are possible now. Nevertheless, the questions that can be definitively answered with N-body simulations are still limited by finite resolution in mass and in distance.²⁹⁾ Since the small-scale structure of the dark matter is essential for the gravitational lensing effects, the simulations using analytic density profiles are important to confirm the results from the N-body simulation, and to investigate new effects that are not found in the N-body simulations.

This paper is organized as follows. In §2.1, we briefly review the gravitational lensing. §2.2 is devoted to describe the clumpy universe model. In §2.3, we show a definition of magnification and the relation between the distance and the magnification. In §3, numerical calculation and our results are illustrated. Finally, §4 is devoted to the conclusions and

summary. Throughout this paper, we use the unit of $G = c = 1$.

§2. Gravitational lensing in a clumpy universe model

2.1. Lens equation

Before describing our settings and calculation method, let us briefly review gravitational lensing. In this paper, we focus on the situation in which thin lens approximation³⁷⁾ is valid. The thin lens models are characterized by the surface mass density $\Sigma(\boldsymbol{\xi})$, where $\boldsymbol{\xi}$ is the impact vector (see Fig. 1). By using the surface mass density $\Sigma(\boldsymbol{\xi})$, the bending angle vector $\hat{\boldsymbol{\alpha}}(\boldsymbol{\xi})$ is given as³⁷⁾

$$\hat{\boldsymbol{\alpha}}(\boldsymbol{\xi}) = 4 \int \frac{(\boldsymbol{\xi} - \boldsymbol{\xi}')\Sigma(\boldsymbol{\xi}')}{|\boldsymbol{\xi} - \boldsymbol{\xi}'|^2} d^2\xi'. \quad (2.1)$$

For convenience, we consider the “straight” line A from a source to the observer and define

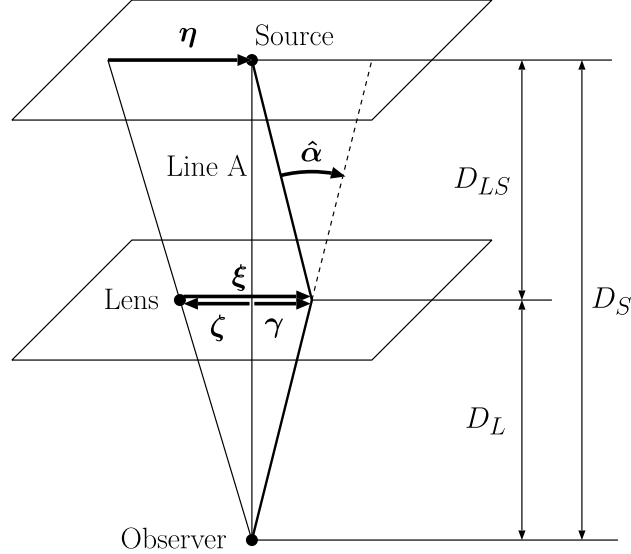


Fig. 1. Geometry of gravitational lensing due to a point-mass lens. The impact vector $\boldsymbol{\xi}$ represents the relative position of a light ray on the lens plane to the lens position, and $\hat{\boldsymbol{\alpha}}$ is a vector whose norm is equal to the bending angle.

the intersection point of A with the lens plane as the origin of the lens position $\boldsymbol{\zeta}$ and the ray position $\boldsymbol{\gamma}$. In the geometrically thin lens approximation, we can regard the vectors $\boldsymbol{\xi}$, $\boldsymbol{\zeta}$, and $\boldsymbol{\gamma}$ on the lens plane.³⁷⁾

We define D_S , D_L , and D_{LS} as the angular diameter distances from the observer to the source, from the observer to the lens, and from the lens to the source, respectively. Using simple trigonometry (see Fig. 1), we find the relation between the source position $\boldsymbol{\eta}$ and $\boldsymbol{\xi}$,

$$\boldsymbol{\eta} = \frac{D_S}{D_L}\boldsymbol{\xi} - D_{LS}\hat{\boldsymbol{\alpha}}(\boldsymbol{\xi}). \quad (2.2)$$

From Eq. (2.2), we have

$$0 = \frac{D_S}{D_L} \gamma - D_{LS} \hat{\alpha}(\gamma - \zeta) \quad (2.3)$$

by using γ instead of ξ and η .

2.2. Clumpy universe model

The clumpy universe model in which we calculate the lensing effects is basically the same as that in Ref. 38). In this clumpy universe model, it is assumed that all matter takes the form of randomly distributed objects and its global property is well described using the Friedmann-Lemaître (FL) universe whose metric is given as

$$ds^2 = -dt^2 + a^2(t) \left(\frac{dr^2}{1 + Kr^2} + r^2 d\Omega^2 \right), \quad (2.4)$$

where $K = 1, 0,$ and $-1,$ and $d\Omega^2$ is the round metric. Hereafter, we will refer to this FL universe as “background universe”.

We assume that the comoving number density ρ_n of the lenses in the clumpy universe is given as

$$\rho_n = \frac{a^3 \rho}{M_L} = \frac{3\Omega_{m0} H_0^2}{8\pi M_L}, \quad (2.5)$$

where $\rho,$ $\Omega_{m0},$ and H_0 are the average mass density, the present values of the total density parameter, and the Hubble parameter, respectively. We consider a past light cone of the observer at $r = 0$ in the background universe, which is parametrized by the redshift z of its null geodesic generator. The comoving volume ΔV of a spherical shell (see Fig. 2) bounded by $r = r(z)$ and $r(z + \Delta z)$ on this light cone is given as

$$\Delta V = \frac{4\pi r^2}{\sqrt{1 + Kr^2}} \frac{dr}{dz} \Delta z. \quad (2.6)$$

Therefore, the number of lenses in this shell is given as

$$\Delta N = \rho_n \Delta V = \frac{3\Omega_{m0} H_0^2 r^2}{2M_L \sqrt{1 + Kr^2}} \frac{dr}{dz} \Delta z. \quad (2.7)$$

We assume dr/dz is the same as the background value,

$$\frac{dr}{dz} = \frac{1}{H_0} \sqrt{\frac{1 + H_0^2 \Omega_{K0} (1+z)^2 D_{FL}^2(z)}{\Omega_{m0} (1+z)^3 - \Omega_{K0} (1+z)^2 + \Omega_{\Lambda 0}}}, \quad (2.8)$$

where $\Omega_{\Lambda 0}$ and $D_{FL}(z)$ are the normalized cosmological constant and the angular diameter distance from the source of the redshift z to the observer in the background universe, respectively, and $\Omega_{K0} = \Omega_{m0} + \Omega_{\Lambda 0} - 1.$

Let us consider a lens plane at the redshift z . We define \mathbf{y} as

$$\mathbf{y} := \frac{\boldsymbol{\zeta}}{\xi_0}, \quad (2.9)$$

where ξ_0 is the Einstein radius given as

$$\xi_0 = \sqrt{4M_L \frac{D_L D_{LS}}{D_S}}. \quad (2.10)$$

\mathbf{y} represents the lens position normalized with the Einstein radius. In addition, we write the absolute values of \mathbf{y} and $\boldsymbol{\zeta}$ as y and ζ , respectively. The average number of lenses in the region $[y, y + \Delta y)$ within the domain $[z, z + \Delta z)$ (see Fig. 2) is given as

$$\frac{2\pi\xi_0^2 y \Delta y}{4\pi a^2 r^2} \Delta N, \quad (2.11)$$

where we have assumed $\zeta \ll r$. This value is equivalent to the probability $p(y, z)\Delta y$ for a

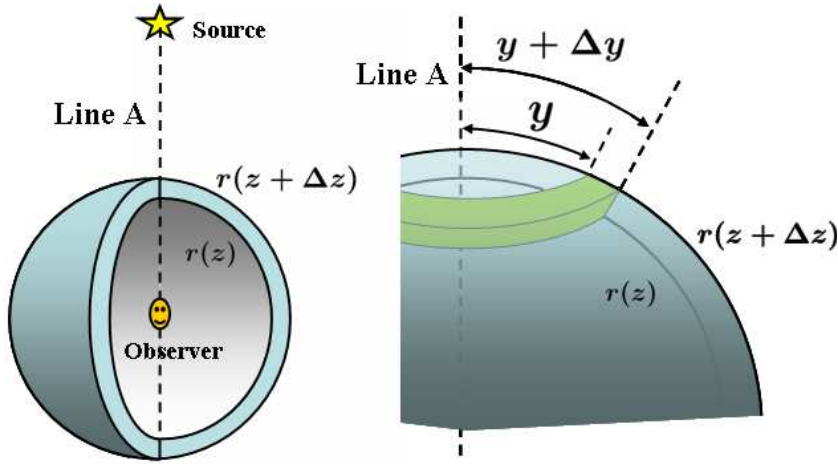


Fig. 2. Figures for §2.2.

light ray to receive lensing effects with impact parameter $[y, y + \Delta y)$ in the domain $[z, z + \Delta z)$. Substituting Eqs. (2.7) and (2.8) into Eq. (2.11) and using Eq. (2.10), we have

$$p(y, z)\Delta y = \frac{3H_0\Omega_{m0}(1+z)^2}{\sqrt{\Omega_{m0}(1+z)^3 - \Omega_{K0}(1+z)^2 + \Omega_{\Lambda0}}} \frac{D_L D_{LS}}{D_S} y \Delta y \Delta z. \quad (2.12)$$

It is seen from Eq. (2.12) that this probability is specified using the model of the background universe.

2.3. Magnification and distance

In this subsection, we discuss the definition of magnification due to lensing and the definition of distance in the clumpy universe model.

First, we consider a point light source that is observed as a single image in a clumpy universe. Magnification μ for a source is defined as

$$\mu = \frac{S}{S_0}, \quad (2.13)$$

where S is the flux actually observed, whereas S_0 is the fictitious flux that would be emitted by the source with the same luminosity and redshift but without lensing effects. If the light ray bundle passes through a spatial section with an area ΔA orthogonal to the ray bundle, using the conservation law of photon number,³⁷⁾ we find

$$\mu = \frac{S}{S_0} = \frac{\Delta A_0}{\Delta A}, \quad (2.14)$$

where ΔA_0 is a sectional area orthogonal to the ray direction in the fictitious propagation process.

The corrected luminosity distance is defined as

$$D' = \left(\frac{\Delta A}{\Delta \Omega_S} \right)^{1/2}, \quad (2.15)$$

where $\Delta \Omega_S$ is the solid angle that subtends a light ray bundle from the point source. The relation between the angular diameter distance D and the corrected luminosity distance D' is given as $D' = (1 + z_S)D$, where z_S is the source redshift.³⁷⁾ Let D_0 denote the angular diameter distance between the source and observer in the case without any lensing effects. Since

$$\left(\frac{\Delta A_0}{\Delta \Omega_S} \right)^{1/2} = (1 + z_S)D_0, \quad (2.16)$$

we obtain

$$D' = \frac{\left(\frac{\Delta A}{\Delta \Omega_S} \right)^{1/2}}{\left(\frac{\Delta A_0}{\Delta \Omega_S} \right)^{1/2}} (1 + z_S)D_0 = (1 + z_S) \frac{D_0}{\sqrt{\mu}}. \quad (2.17)$$

Therefore, we can define the observed angular diameter distance D_A as

$$D_A = \frac{D_0}{\sqrt{\mu}}. \quad (2.18)$$

Next, let us consider the case of multiple images. The magnification $\mu_{(p)}$ of the p -th image of a source is defined as

$$\mu_{(p)} = \frac{S_{(p)}}{S_0}, \quad (2.19)$$

where $S_{(p)}$ is the flux of the p -th image. In this study, we assume that multiple images can not be distinguished from each other owing to the limitation of the resolution, and we can observe only the total flux of light rays. Then the observed magnification μ is given as

$$\mu = \frac{\sum_p S_{(p)}}{S_0} = \sum_p \mu_{(p)}, \quad (2.20)$$

and we define the observed angular diameter distance as

$$D_A = \frac{D_0}{\sqrt{\sum_p \mu_{(p)}}}. \quad (2.21)$$

In terms of the angular diameter distance, the magnification is written as

$$\mu = \frac{D_0^2}{D_A^2}. \quad (2.22)$$

The angular diameter distance in gravitational lensing is discussed for many years.^{45), 46)} The angular diameter distance in the FL universe, D_{FL} , and the Dyer-Roeder distance,^{40), 41)} D_{DR} , are commonly used. The Dyer-Roeder distance is the distance in the under dense region in the inhomogeneous matter distribution. It depends on the smoothness parameter α , which is the ratio of the smoothly distributed matter density except for clumps to the mean energy density ρ for all matter in the universe. When $\alpha = 1$, the universe becomes the FL universe and D_{DR} agrees with D_{FL} . When $\alpha = 0$, all matter takes the form of clumps, and in such a case, the Dyer-Roeder distance is the distance in an empty region in the clumpy universe.

In our work, unlensed angular diameter distance D_0 should be appropriately chosen so as to be consistent with the situations of our present interest as below.⁵¹⁾ We are investigating the lensing effects of SNe, whose linear extent is much smaller than the scales in which density inhomogeneities are linear or quasi-linear. Then, the matter distribution might be highly clumpy, and the under dense region might be almost empty.

In this situation, we expect that the focusing effects the light ray receives are minimal, and that the angular diameter distance agrees with the Dyer-Roeder distance, because the light rays do not receive any lensing effects between the lens planes. This is consistent with the numerical simulations by Holz & Wald²⁷⁾ and Kozaki.⁵²⁾ Holz & Wald²⁷⁾ discussed the angular diameter distance in the universe that consists of many small balls. Kozaki⁵²⁾ calculated the distance-redshift relations in the Swiss-cheese universe model, that is an exact solution of the Einstein equation. In this paper, we adopt the Dyer-Roeder distance D_{DR} with $\alpha = 0$ as D_0 and for the distance between each lens plane which has positive definite surface mass density $\Sigma(\xi)$. Hereafter, we drop ‘‘with $\alpha = 0$ ’’, and simply call this distance the ‘‘Dyer-Roeder distance D_{DR} ’’.

In Refs.49),50), it is shown that the observed distance after the multiple lensing effects sometimes becomes longer than the DR distance. In such cases, α becomes negative. In our simulation, we do not treat such a case and use the Dyer-Roeder distance as the angular diameter distance. To understand such situations, we need further studies.

If inhomogeneities are so small that these are regarded as linear or quasi-linear perturbations in the homogeneous and isotropic universe, perturbative treatments seem to be better in gravitational lensing. In such perturbative treatments, the unlensed distance D_0 is the angular diameter distance in the FL universe D_{FL} . Light rays are perturbed by the lensing effects of the inhomogeneity. In this sense, the (de)magnification is often defined as $\tilde{\mu} := D_{FL}^2/D_A^2$ in weak lensing analyses and ray shooting calculations.^{42)–44)} In their works, the surface mass density of each lens plane is not positive definite, namely, the under dense regions have negative mass density. The relation between μ and $\tilde{\mu}$ is given as

$$\tilde{\mu} = \mu \frac{D_{FL}^2}{D_{DR}^2}. \quad (2.23)$$

§3. Numerical calculation and results

3.1. Numerical methods and the density profiles of lens models

In this study, we use the numerical method proposed by Rauch.⁷⁾ We compute lens mappings using the multiple lens plane method.³⁷⁾ We ignore the lensing effects coming from clumps far from the ray. We search for the position of images on the field of view using the Newton-Raphson method. Summing up the magnifications of all images, we obtain the total magnification. The concrete description about the method is in Ref.38) and we review it in Appendix A.

In the simulations, we assume that clumps in the universe are transparent to light rays. We also assume that clumps are axisymmetric, and the axes of symmetry of clumps are identical with the line of sight. Each of these clumps has the mass M_L and the “size” R . We consider the following three lens models: *)

(a) Homogeneous disk:

$$\Sigma(\xi) = \begin{cases} \frac{M_L}{\pi R^2} & \text{for } \xi < R, \\ 0 & \text{for } \xi \geq R. \end{cases} \quad (3.1)$$

*) Numerical calculations have been performed also for homogeneous sphere: $\Sigma(\xi) = \frac{3M_L}{2\pi R^2} (1 - \xi^2/R^2)^{1/2}$ and power low tail model: $\Sigma(\xi) = \frac{M_L}{\pi R^2(1+\xi^2/R^2)^2}$. The results are qualitatively the same as those of the lens models (a) and (b). We do not show these results in this paper.

(b) Log cusp model:

$$\Sigma(\xi) = \begin{cases} \frac{2M_L}{\pi R^2} \ln \frac{R}{\xi} & \text{for } \xi < R, \\ 0 & \text{for } \xi \geq R. \end{cases} \quad (3.2)$$

(c) $1/\xi$ cusp model (Singular Isothermal Sphere):

$$\Sigma(\xi) = \begin{cases} \frac{M_L}{2\pi R^2} \frac{R}{\xi} & \text{for } \xi < R, \\ 0 & \text{for } \xi \geq R. \end{cases} \quad (3.3)$$

The degree of the density concentration at the center of the log cusp model (b) is equivalent to the spherical Navarro-Frenk-White (NFW)³⁹⁾ lens model in which the mass density, ρ , is inversely proportional to the radius.

The surface mass density of all our lens models can be written in the form,

$$\Sigma(\xi) \propto \frac{M_L}{R^2} F\left(\frac{R}{\xi}\right), \quad (3.4)$$

where $F(R/\xi)$ is a function of R/ξ , ξ is the distance from the axis of symmetry on the lens plane, and $\Sigma(\xi)$ is the surface mass density. We assume that the total mass of each lens object $M_L = 2\pi \int_0^\infty \xi \Sigma(\xi) d\xi$ is finite. If we use Eq. (3.4) and use the calculation method written in Appendix A, we find that the magnification distribution does not change if we scale the parameter in the manner $R \rightarrow CR$ and $M_L \rightarrow C^2 M_L$, where C is an arbitrary constant. This means that the magnification depends only on the parameter $R/\sqrt{M_L}$. A proof of this fact is given in Appendix A.

3.2. MPDFs

We first consider the cases in which $R/\sqrt{M_L} = \text{constant}$, and investigate the dependence of MPDFs on lens models and on the value of $R/\sqrt{M_L}$. The magnification is stochastic owing to the randomness of the lens distribution. We numerically generate 100,000 samples of magnification for each lens model characterized by the parameter $R/\sqrt{M_L}$. In our calculations, we use the same realization of the lens distribution for each model. The MPDFs given as results of these calculations are shown in Figs. 3-5.

In Fig. 3, MPDFs for case (a) are depicted. There are a few frames in which two or three peaks appear in an MPDF. The largest peak and the second or third largest peak in the case of $(z_S, R\sqrt{H_0/M_L}) = (0.4, 6)$, $(1.2, 2)$, and $(2, 2)$ can be explained as the effect of the small lensing probability. When the lensing probability is relatively small, most of the light rays do not experience the lensing. In this case, it is thus expected that the MPDF has a peak at 1. This is because, in our definition of the magnification, when a light ray does not experience the lensing, the magnification is 1. When the light rays experience the lensing effect only once, the magnification typically becomes $\mu \sim R^4/(R^2 - M_L D_S)^2$ as shown in

Appendix B. As a result, we find the second peak around $\mu \sim R^4/(R^2 - M_L D_S)^2$, which can be seen in Fig. 3.

In Figs. 3-5, we find that, in many cases, MPDFs can be fitted using the gamma distribution $f(\mu - 1; k, \theta)$ defined as

$$f(\mu - 1; k, \theta) = (\mu - 1)^{k-1} \frac{e^{-(\mu-1)/\theta}}{\theta^k \Gamma(k)}, \quad (3.5)$$

where $k > 0$ and $\theta > 0$ are called the shape parameter and scale parameter, respectively, and $\Gamma(k)$ is the gamma function. In these figures, we depict the gamma distributions that fit the MPDFs. The parameters of the gamma distributions are determined by the maximum likelihood method as follows. We assume that the numerically generated magnifications are independent of each other and identically distributed random variables that obey the gamma distribution. The logarithm of the likelihood function \mathcal{L} for N samples of the magnification, (μ_1, \dots, μ_N) is given as

$$\ln \mathcal{L}(k, \theta) = \sum_{i=1}^N \ln f(\mu_i - 1, k, \theta). \quad (3.6)$$

The shape parameter and the scale parameter are related to the mean μ_m and variance σ of the gamma distribution as follows:

$$\mu_m = k\theta + 1, \quad (3.7)$$

$$\sigma^2 = k\theta^2. \quad (3.8)$$

The maximum likelihood estimates of the shape and scale parameters, \hat{k} and $\hat{\theta}$, are obtained by solving the equations,

$$\left. \frac{\partial}{\partial \theta} \ln \mathcal{L}(k, \theta) \right|_{k=\hat{k}, \theta=\hat{\theta}} = 0, \quad \left. \frac{\partial}{\partial k} \ln \mathcal{L}(k, \theta) \right|_{k=\hat{k}, \theta=\hat{\theta}} = 0. \quad (3.9)$$

The means $\langle \mu \rangle$ and variances of the numerically generated MPDFs are plotted as functions of z_S in Figs. 6 and 7. The shape parameter k and the scale parameter θ of the gamma distributions that fit the MPDFs are also plotted as functions of z_S in Figs. 8 and 9. As explicitly shown in Fig. 6, $\langle \mu \rangle$ is almost equal to D_{DR}^2/D_{FL}^2 . The deviations are smaller than 1% in all cases.

In the case of $z_S = 1.2$ and $z_S = 2.0$ for the lens models (a) (see Fig. 3), the gamma distributions fit well the MPDFs for $R/\sqrt{M_L} = 6H_0^{-1/2}$, $10H_0^{-1/2}$ but do not for $R/\sqrt{M_L} = 2H_0^{-1/2}$. In the case of model (b) and $z_S \geq 1.2$ (Fig. 4), the gamma distribution fits well the MPDFs for $R/\sqrt{M_L} \geq 2H_0^{-1/2}$. In contrast, the gamma distributions do not fit

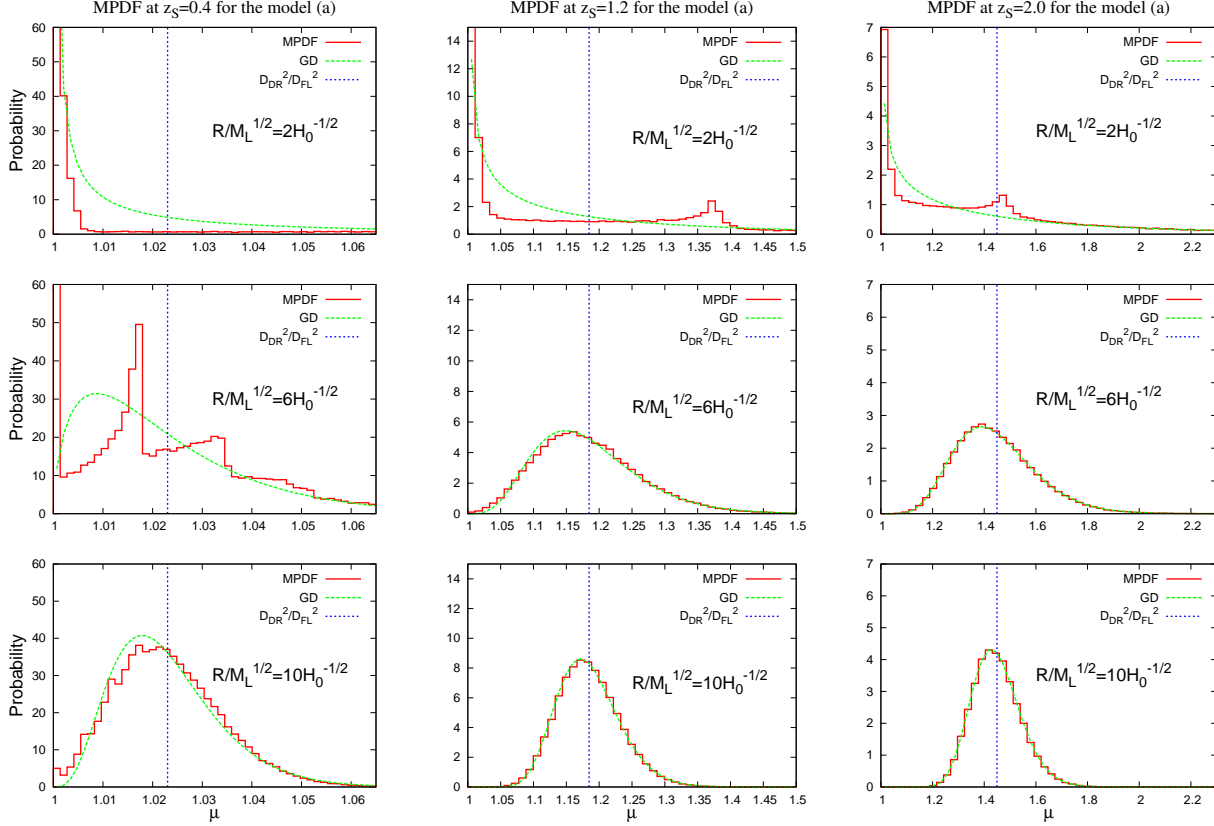


Fig. 3. MPDFs for the lens model (a) at $z_S = 0.4, 1.2,$ and 2.0 are shown on the left, center, and right lines, respectively. The smooth lines are the gamma distributions that fit the MPDFs.

well the MPDFs in all cases for lens model (c) (see Fig. 5). The lens model (c) has the steepest density profile at the center among the lens models considered here. The reason for the deviation from the gamma distributions seems to come from this steep density profile. This is consistent with the fact that, in the case of the point mass lens model, the gamma distributions do not fit the MPDFs. *) This also suggests that, even in models (a) and (b), if we set $R/\sqrt{M_L}$ sufficiently smaller than $R/\sqrt{M_L} = 2H_0^{-1/2}$, the gamma distributions do not fit the MPDFs irrespective of z_S .

Let us discuss the z_S dependence of MPDFs. We consider the case of $R/\sqrt{M_L} = 6H_0^{-1/2}$ for the lens model (a). While the gamma distribution fits well the MPDF at $z_S = 2$, it does not at $z_S = 0.4$. The most significant difference between these two cases is the number of lensing effects the light rays experience. Hence, our results suggest that, in order for a MPDF to be fitted well by the gamma distribution, the light rays need to pass through near the clumps frequently. However, to clarify the condition for the realization of the gamma

*) In the case of point mass lens, the magnification probability behaves $\sim \mu^{-3}$ when $\mu \gg 1$ (see, e.g., Ref.53) or 54)).

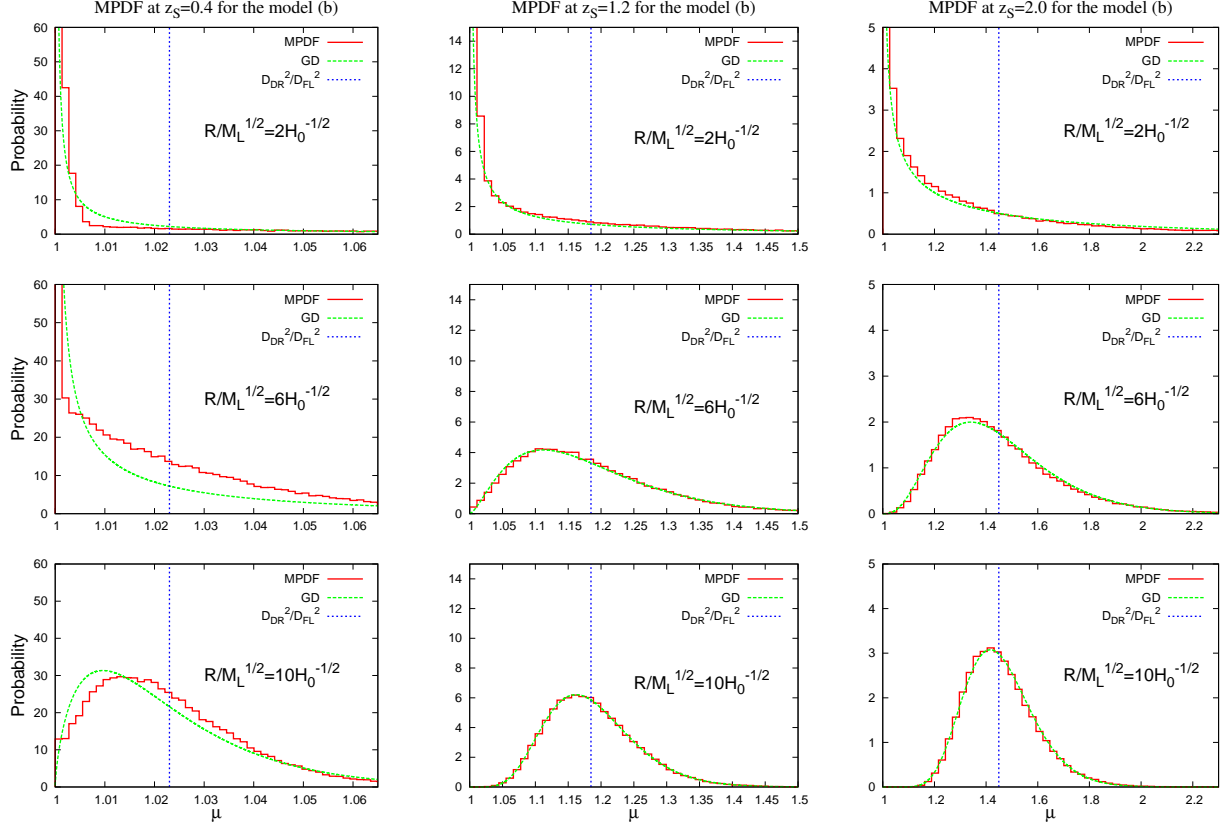


Fig. 4. Same as Fig. 3, but for the lens model (b).

distribution more precisely, much more detailed investigations are required.

The above results suggest that if lens models have sufficiently gradual density profiles, the MPDF is universally well fitted using the gamma distribution. To obtain further evidence for this hypothesis, we calculate an MPDF in the case when the value of $R/\sqrt{M_L}$ is not constant. We assume the lens model (b) in which $R\sqrt{H_0/M_L}$ of each lens randomly takes a value within $6 \leq R\sqrt{H_0/M_L} \leq 10$, and that the redshift of the light source is given as $z_S = 1.2$. The MPDF is shown in Fig. 10. One can find that MPDF is fitted well by the gamma distribution even if the value of $R/\sqrt{M_L}$ is distributed. This fact might not be surprising, because the effect of changing the value of $R/\sqrt{M_L}$ is similar to the effect of changing the impact parameter of a light ray from a lens. Both effects produce the change in the magnification. The shape parameter and the scale parameter become $\theta = 0.041$ and $k = 4.5$, respectively. These are intermediate values between those in the cases of $R/\sqrt{M_L} = 6H_0^{-1/2}$ and $R/\sqrt{M_L} = 10H_0^{-1/2}$ for the lens model (b).

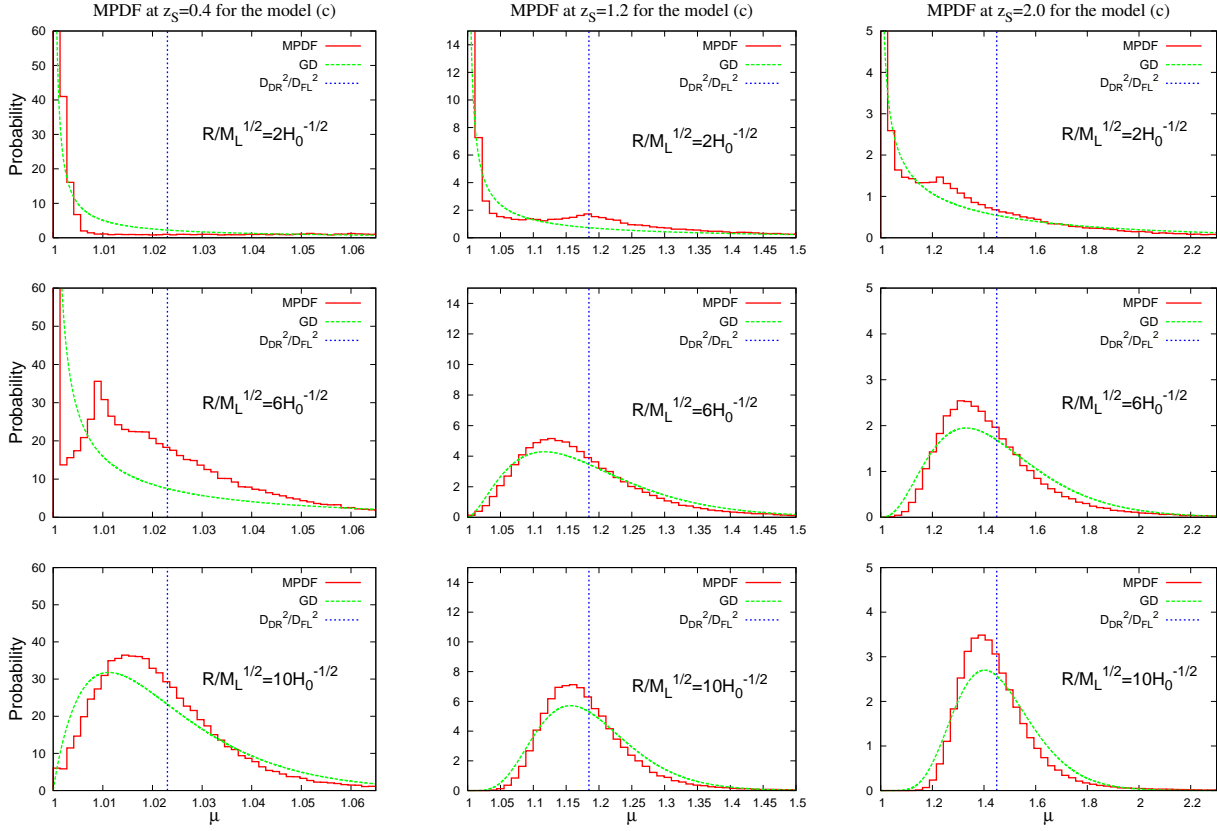


Fig. 5. Same as Fig. 3, but for the lens model (c).

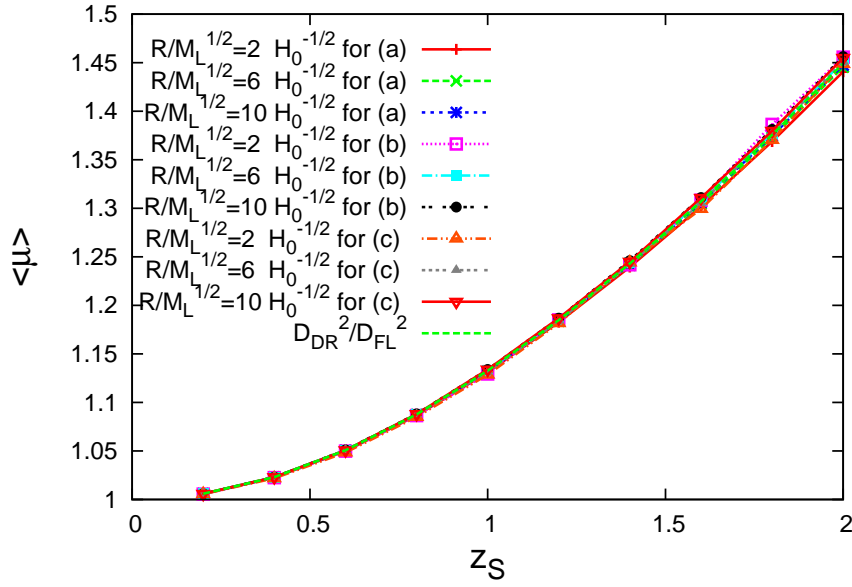


Fig. 6. The mean values of the magnification μ are depicted as functions of the source redshift.

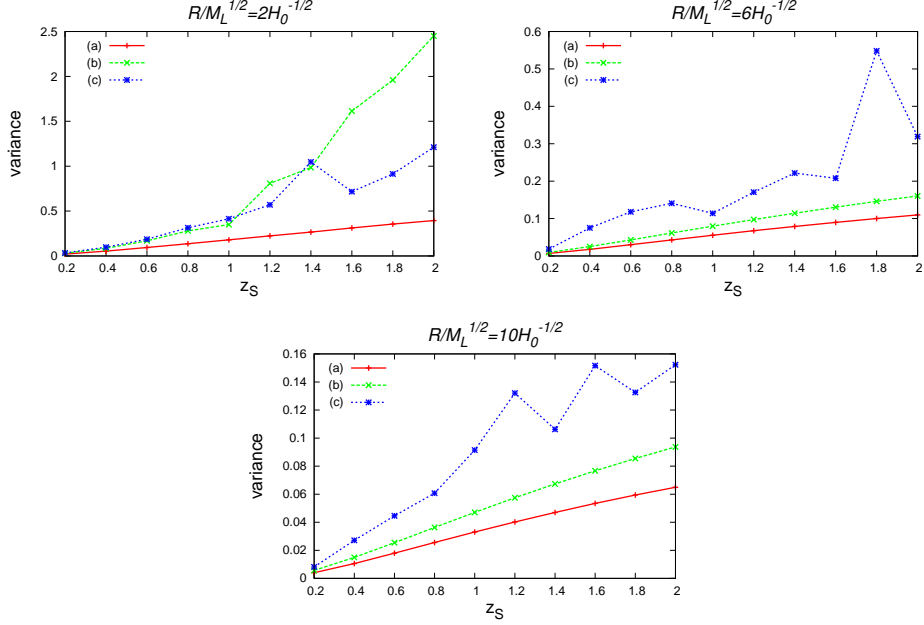


Fig. 7. The variances are depicted as functions of the source redshift.

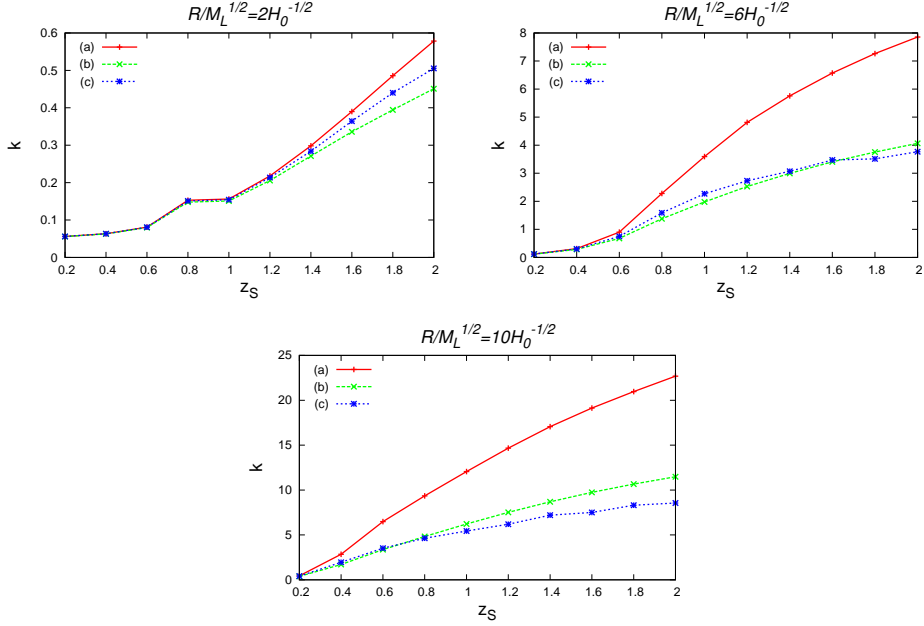


Fig. 8. The shape parameters k are depicted as functions of the source redshift.

3.3. χ^2 -test

The discussions in §3.2 suggest that we may obtain the information about the slope of dark matter density profiles at the central cusp from the Type Ia supernovae observation. To clarify this possibility, we investigate the relation between the goodness of fitting of the MPDFs to the gamma distributions and the steepness of the central density profile using

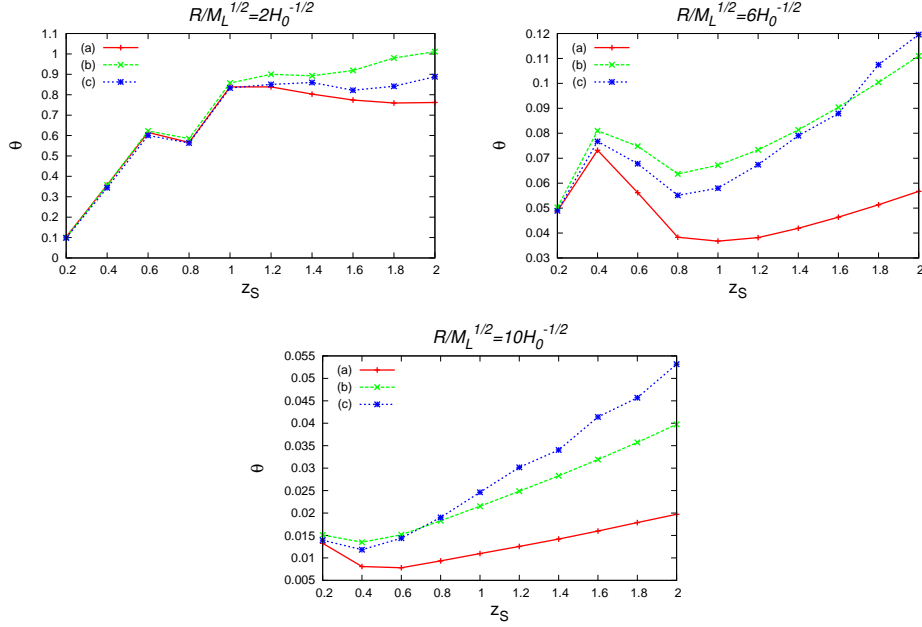


Fig. 9. The scale parameter θ is depicted as a function of the source redshift.

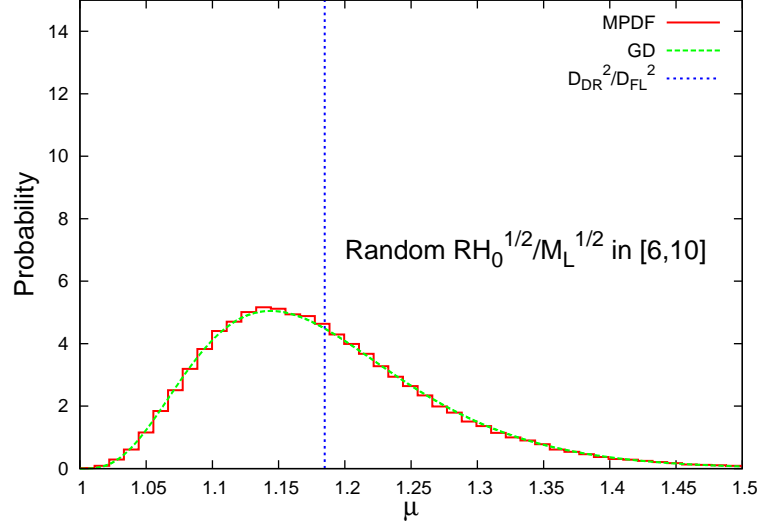


Fig. 10. MPDF for the lens model (b) at $z_S = 1.2$ is shown. Values of $R\sqrt{H_0/M_L}$ of clumps are distributed uniformly within $6 \leq R\sqrt{H_0/M_L} \leq 10$. The smooth lines are the gamma distributions that fit the MPDFs.

the power law cusp lens model defined as

$$\Sigma(\xi) = \begin{cases} \frac{(2-n)M_L}{2\pi R^2} \left(\frac{R}{\xi}\right)^n & \text{for } \xi < R, \\ 0 & \text{for } \xi \geq R. \end{cases} \quad (3.10)$$

This lens model includes the lens models (a) and (c) in §3.2 as the special cases. If we set $n = 0$ or 1 in the Eq. (3.10), this model becomes model (a) or (c), respectively.

We use the value of χ^2 as an indicator of the goodness of fitting to the gamma distribution. Here, χ^2 is defined as follows. The values of the magnification μ of each sample are labelled with i ($i = 1, \dots, N$) so that μ_i satisfies the relation, $\mu_1 \leq \mu_2 \leq \dots \leq \mu_N$. We divide the region $\mu \geq 1$ into p bins. In this paper, we set $p = 15$. The boundaries of the bins are expressed as ν_j ($j = 0, \dots, p - 1$), which satisfy the relation, $\nu_0 < \nu_1 < \dots < \nu_{p-1}$, where $\nu_0 = 1$. We define $\nu_1 = (\mu_m + \mu_{m+1})/2$ so that there are m samples in the 1st bin. In the same way, we define $\nu_{p-1} = (\mu_{N-m} + \mu_{N-m+1})/2$ so that there are m samples in the p th bin. The values of ν_i from $i = 2$ to $p - 2$ are determined by even spacing. Namely, they are given as

$$\nu_j = \nu_1 + (j - 1)\Delta\nu, \quad (j = 2, \dots, p - 1) \quad (3.11)$$

$$\Delta\nu = (\nu_{p-1} - \nu_1)/(p - 2). \quad (3.12)$$

The value of m is determined such that each bin has a sufficiently large number of samples.

For j -th bin, we have the number of samples in this bin, m_j , and the expected number of samples, e_j , derived from the gamma distributions. We then define the value of χ^2 as

$$\chi^2 = -2 \sum_{i=1}^{15} m_i \log \frac{e_i}{m_i}. \quad (3.13)$$

In Fig. 11, we depict the value of χ^2 as the function of the steepness n of the density profile, where $N = 100,000$, and we have set $R/\sqrt{M_L} = 10H_0^{-1/2}$, $z_S = 1.2$, and $m = 100$. The

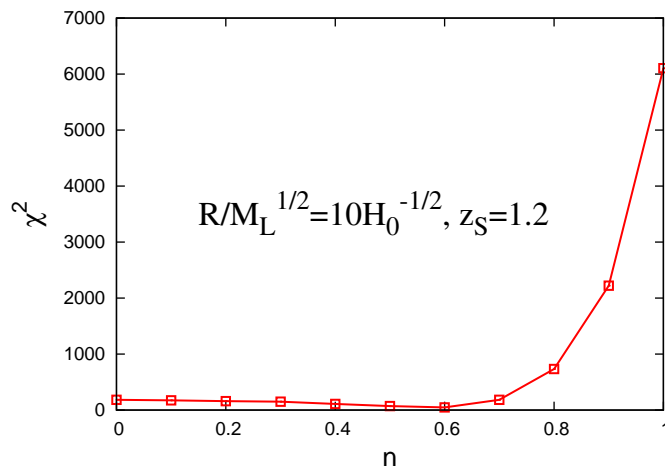


Fig. 11. The value of χ^2 is depicted as the function of power n , where we set $R/\sqrt{M_L} = 10H_0^{-1/2}$ and $z_S = 1.2$.

value of χ^2 increases rapidly with n if $n > 0.6$.

SNAP will be able to find the order of 1000 SNe per year within the redshift ~ 1 . To simulate such situation, we divide the 100,000 samples into 100 datasets of 1000 samples, and

perform the χ^2 -test for each dataset. In this case, we set $m = 10$. When the value of χ^2 is larger than a certain threshold, we judge that the MPDF cannot be fitted using the gamma distribution. The threshold is determined such that there is only a 5 % probability that the dataset generated from the gamma distribution is rejected. The relation between the rate of rejection and the value of n is shown in Table I. We find that if $n \leq 0.7$, the rejection rate is around 10% or less than that. However, if $n \geq 0.8$, the rejection rate increases rapidly. This result suggests that we may constrain the slope of the dark matter density profile at the central cusp from the goodness of the fitting of the gamma distribution to the MPDF.

Table I. The rate of rejection through the χ^2 -test with 1000 samples is shown in this table.

Power n	0	0.1	0.2	0.3	0.4	0.5	0.6	0.7	0.8	0.9	1.0
Rate of rejection	0.1	0.06	0.06	0.05	0.12	0.14	0.07	0.11	0.27	0.82	0.97

§4. Summary and conclusions

We have studied lensing effects on observations of point sources such as Type Ia supernovae by the Monte-Carlo simulation. It has been assumed that all matter in the universe takes the form of randomly distributed objects each of which has finite size and transparent to light rays. In addition, we have assumed that each of the lens objects is axially symmetric along the line of sight. We have found analytically that the magnification probability distribution functions (MPDFs) depend on the mass M_L and the size R of a lens object only through the form $R/\sqrt{M_L}$. We have calculated MPDFs for various values of the source redshift and $R/\sqrt{M_L}$. We found that the resultant MPDFs can be categorized into two groups according to whether the gamma distributions fit well the MPDFs or not. In the case of the lens models that have smooth density profiles, the gamma distributions fit well the MPDFs if $R\sqrt{H_0/M_L}$ is sufficiently large. Furthermore, we have found that this result holds in the lens model that has the same degree of density concentration at the center as the Navarro-Frenk-White (NFW) lens model. In contrast, the gamma distributions do not fit well the MPDFs for any value of $R/\sqrt{M_L}$ in the case of the singular isothermal sphere (SIS) lens model. These results suggest that we might be able to distinguish the NFW lens model from the SIS lens model on the basis of MPDFs.

We have shown that MPDF is well fitted using the gamma distribution even if the value of $R/\sqrt{M_L}$ is uniformly distributed within $6 \leq R/\sqrt{M_L} \leq 10$ in the case of lens model (b). This result suggests that MPDF is universally well fitted using the gamma distribution if lens models have sufficiently gradual density profiles. To obtain further evidence for this hypothesis, we need to clarify the effect of the distribution of $R/\sqrt{M_L}$ in more detail. This

is one of our future works.

We introduced the power law cusp lens model, and we investigated the dependence of the goodness of the fitting with the gamma distribution on the power n , which represents the steepness of the cusp at the center. We have generated 100,000 samples of magnification in the Monte-Carlo simulations. We divided the 100,000 samples into 100 datasets of 1000 samples, and performed the χ^2 -test for each dataset, since the same analysis might be possible for the observational data of SNAP. Then, we found the significant difference in the rate of rejection between $n \leq 0.7$ and $n \geq 0.8$. This result suggests that we may obtain the information about a slope of the density profiles of the central cusp of dark matter using MPDF of Type Ia supernovae.

A mathematical explanation of the reason why we obtain the gamma distribution is unavailable now. In Refs.(22), (33), (55), and (25), analytic fitting functions different from ours for MPDF are proposed. The relation between our analytic fitting function and those should be studied. We note that we need to examine the effect of simplifications carried out in this study, before we compare our results with observations. For example, we have assumed that there are no spatial correlations of the distribution of the clumps. The effect of the spatial correlation of the clumps should be clarified. We leave these issues as our future works.

The density profile of dark matter halos is a hot topic in astrophysics both theoretically and observationally (See e.g. Ref.29)). Our results suggest that, although there are some simplifications in comparison with realistic situations of our universe, the statistical gravitational lensing effect may shed a new light on the observational investigation of the density profile of dark matter halos.

Acknowledgements

We would like to acknowledge the helpful advice of Professor M. Sasaki and Dr. H. Kozaki. C. Yoo was supported by the 21st COE program “Constitution of wide-angle mathematical basis focused on knots” from the Japan Ministry of Education, Culture, Sports, Science and Technology. H.T’s work was supported in part by JSPS, KAKENHI, Nos.16540251 and 20540271. This work was supported in part by a JSPS Grant-in-Aid for Scientific Research (B), No. 17340075.

Appendix A

— Calculation Method —

To calculate magnification factors, we use the multiple lens-plane method.³⁷⁾ We consider the “straight” line A from the source to the observer, and we put N lens planes between them

so that the straight line A intersects vertically. We denote lens planes from the observer to the source sequentially as $\Sigma_1, \Sigma_2, \dots, \Sigma_N$. For convenience, we label the source plane that is also orthogonal to the line A as Σ_{N+1} . On each lens plane, say Σ_i , the lens position ζ_i and the ray position γ_i are specified with respect to the intersection point of A .

Suppose lens positions ζ_i ($i = 1, \dots, N$) are given. When we emanate a ray with a ray position γ_1 on Σ_1 , the lens position on the j -th lens plane Σ_j ($j \leq N + 1$) is recursively given as follows

$$\gamma_j = \frac{D_j}{D_1} \gamma_1 - \sum_{i=1}^{j-1} D_{ij} \hat{\alpha}(\gamma_i - \zeta_i), \quad (\text{A}\cdot 1)$$

where D_{ij} is the DR distance from the i ($< j$)-th plane to the j -th plane. The right hand side of equation (A.1) also includes ray positions $\gamma_2, \dots, \gamma_{j-1}$. Thus, we must calculate the ray positions $\gamma_2, \dots, \gamma_{j-1}$ to obtain the ray position γ_j . For later convenience, we specify the ray positions and lens positions using the following dimensionless quantities:

$$\mathbf{u}_i := \frac{\gamma_i}{D_i}, \quad (\text{A}\cdot 2)$$

$$\mathbf{q}_i := \frac{\zeta_i}{D_i}. \quad (\text{A}\cdot 3)$$

Equation (A.1) is written as

$$\mathbf{u}_j = \mathbf{u}_1 - \sum_{i=1}^{j-1} \beta_{ij} \alpha(\mathbf{u}_i - \mathbf{q}_i), \quad (\text{A}\cdot 4)$$

where

$$\beta_{ij} := \frac{D_{ij} D_S}{D_j D_{iS}} \quad (\text{A}\cdot 5)$$

and

$$\alpha(\mathbf{u}_i - \mathbf{q}_i) := \frac{D_{iS}}{D_S} \hat{\alpha}(\gamma_i - \zeta_i). \quad (\text{A}\cdot 6)$$

In the case of the multiple lensing effect, multiple images appear in general. We specify the paths from the source to the observer using their ray positions, say $\mathbf{v}_{(p)}$, on the first lens plane. For a path $\mathbf{v}_{(p)}$, the magnification $\mu_{(p)}$ is defined as

$$\mu_{(p)} = \frac{1}{\det \mathcal{A}_{(p)}}, \quad (\text{A}\cdot 7)$$

where $\mathcal{A}_{(p)}$ is the Jacobian matrix of the lens mapping:

$$\begin{aligned} \mathcal{A}_{(p)} &= \left. \frac{\partial \mathbf{u}_{N+1}}{\partial \mathbf{u}_1} \right|_{\mathbf{u}_1 = \mathbf{v}_{(p)}} \\ &= \mathcal{I} - \sum_{i=1}^N \beta_{i,N+1} \frac{\partial \alpha(\mathbf{u}_i - \mathbf{q}_i)}{\partial \mathbf{u}_i} \frac{\partial \mathbf{u}_i}{\partial \mathbf{u}_1} \Big|_{\mathbf{u}_1 = \mathbf{v}_{(p)}}. \end{aligned} \quad (\text{A}\cdot 8)$$

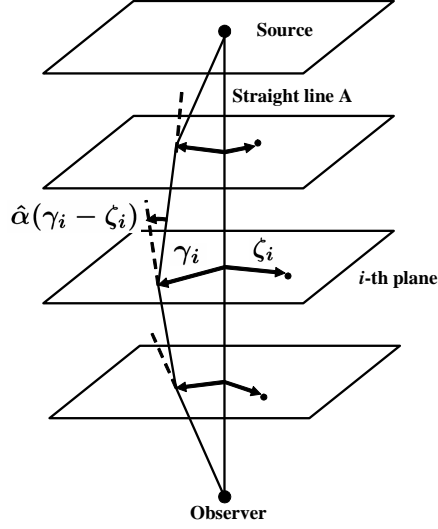


Fig. 12. The definitions of vectors α_j , ζ_j , and γ_j are given here.

We obtain the following result.

Proposition. *The magnification probability distribution function for the identical lens objects is invariant under the following constant rescaling of the linear extent R and the mass M_L of the lens object*

$$R \rightarrow CR \quad \text{and} \quad M_L \rightarrow C^2 M_L, \quad (\text{A}\cdot 9)$$

if the surface mass densities of the lens objects are given in the form of Eq.(3.4).

Proof. The parameter ξ_0 becomes $C\xi_0$ through the changes of the parameters (A.9) due to its definition (2.10). Hence, we find from Eq. (2.12) that the density $p(y, z)$ of lenses in (y, z) space is unchanged through the replacement (A.9), if ζ is also replaced by $C\zeta$; hereafter we assume so.

Substituting Eq. (3.4) into Eq. (2.1), we have

$$\hat{\alpha}(\boldsymbol{\xi}) = \text{Const} \times \frac{4M_L}{R^2} \int_{\xi' \leq R} \frac{(\boldsymbol{\xi} - \boldsymbol{\xi}') F(R/\xi')}{|\boldsymbol{\xi} - \boldsymbol{\xi}'|^2} d^2 \xi'. \quad (\text{A}\cdot 10)$$

For the changes in the parameters (A.9), $\hat{\alpha}$ changes in the manner

$$\begin{aligned} \hat{\alpha}(\boldsymbol{\xi}) &\longrightarrow \text{Const} \times \frac{4M_L}{R^2} \int_{\xi' \leq CR} \frac{(\boldsymbol{\xi} - \boldsymbol{\xi}') F(CR/\xi')}{|\boldsymbol{\xi} - \boldsymbol{\xi}'|^2} d^2 \xi' \\ &= \text{Const} \times \frac{4M_L}{R^2} \int_{\bar{\xi} \leq R} \frac{(\boldsymbol{\xi} - C\bar{\boldsymbol{\xi}}) F(R/\bar{\xi})}{|\boldsymbol{\xi} - C\bar{\boldsymbol{\xi}}|^2} C^2 d^2 \bar{\xi} \\ &= C \hat{\alpha}(C^{-1} \boldsymbol{\xi}), \end{aligned} \quad (\text{A}\cdot 11)$$

where in the second line, we have replaced the variable of integration $\boldsymbol{\xi}'$ by $\bar{\boldsymbol{\xi}} = C^{-1} \boldsymbol{\xi}'$.

The solution of Eq. (A.1) with the parameters changed as Eq. (A.9) is denoted by $\tilde{\gamma}_j$. By using Eq. (A.11), the equations satisfied by $\tilde{\gamma}_j$ are given as

$$\tilde{\gamma}_j = \frac{D_j}{D_1} \tilde{\gamma}_1 - \sum_{i=1}^{j-1} D_{ij} C \hat{\alpha} (C^{-1} [\tilde{\gamma}_i - C \zeta_i]). \quad (\text{A.12})$$

It is easily confirmed that $\tilde{\gamma}_j = C \gamma_j$ is the solution for the above equation, where γ_j is the solution of Eq. (A.1). Thus, for the changes in the parameters of lens objects (A.9), we have the following scaling law

$$\mathbf{u}_j \longrightarrow C \mathbf{u}_j, \quad (\text{A.13})$$

(see Eq. (A.2)). Since the Jacobian matrix $\mathcal{A}_{(p)}$ is invariant for the constant rescaling (A.13) due to definition (A.8), we eventually find that the Jacobian matrix $\mathcal{A}_{(p)}$ does not change through the replacement (A.9). This result means that the magnification $\mu_{(p)}$ is invariant for the change in parameters in the form of (A.9) and thus the magnification probability distribution function is also invariant for (A.9). \square

The above result guarantees that the MPDF depends on only the parameter $R/\sqrt{M_L}$.

We randomly put lenses so that the distribution of those is consistent with equation (2.12). First, we divide the spherical region $z < z_S$ into N concentric spherical shells each of which is bounded by two spheres $z = z_i - \Delta z/2$ and $z = z_i + \Delta z/2$. We take into account only the nearest lens in each shell. We find from equation (2.12) that in the i -th shell $z_i - \Delta z/2 < z < z_i + \Delta z/2$ there is one point mass on average within the region $y \leq Y_i$, where

$$\int_0^{Y_i} p(y, z_i) dy = 1. \quad (\text{A.14})$$

Therefore we randomly put a point mass within the region $y \leq Y_i$ in the i -th shell. We can neglect the lensing effects of the clumps that are so far from the ray that they do not affect the magnification. We set an upper bound y_{\max} ($< Y_i$) to the lens position, and take account of lensing effects due to the lenses in the region $y < y_{\max}$. We have set the value of y_{\max} as ^{*)}

$$y_{\max} = \max \left\{ 5, \frac{R}{\xi_0} + 1 \right\}. \quad (\text{A.15})$$

Next, we show the method to find paths from the source to the observer: $\mathbf{v}_{(p)}$. When lens positions are given, the dimensionless ray position \mathbf{u}_{N+1} on the source plane Σ_{N+1} is given as a function of only the ray position \mathbf{u}_1 on the first lens plane Σ_1 ;

$$\mathbf{u}_{N+1} = \mathbf{f}(\mathbf{u}_1). \quad (\text{A.16})$$

^{*)} We have determined the value of y_{\max} as sufficiently large so that $\langle \mu \rangle \simeq D_{DR}^2/D_{FL}^2$ in the case of the power law tail lens model.

Therefore, to find $\mathbf{v}_{(p)}$, we solve the equation:

$$\mathbf{u}_{N+1}(\mathbf{u}_1) = 0. \quad (\text{A}\cdot 17)$$

We find the roots of equation (A-17) by the Newton-Raphson method. The technical details can be seen in Ref.7).

Appendix B

—— Typical Value of the Magnification for the Lens Model (a) ——

In the case of the lens model (a), from Eq. (2.1), the bending angle vector $\hat{\boldsymbol{\alpha}}(\boldsymbol{\xi})$ is given as

$$\hat{\boldsymbol{\alpha}}(\boldsymbol{\xi}) = \frac{4M_L}{R^2} \boldsymbol{\xi}. \quad (\text{B}\cdot 1)$$

Since the magnification μ due to only one lens plane is given as

$$\mu = \left| \det \left(\frac{\partial \boldsymbol{\eta}}{\partial \boldsymbol{\xi}} \right) \right|^{-1} \frac{D_S^2}{D_L^2}, \quad (\text{B}\cdot 2)$$

we have

$$\mu = \frac{R^4}{\left(R^2 - \frac{4M_L D_L D_{LS}}{D_S} \right)^2} \quad (\text{B}\cdot 3)$$

for the lens model (a) from Eq. (2.2). Using D_S instead of $2D_L$ or $2D_{LS}$, we have

$$\mu \sim \frac{R^4}{(R^2 - M_L D_S)^2}. \quad (\text{B}\cdot 4)$$

References

- 1) S. Perlmutter et al., *Astrophys. J.* **517** (1999), 565.
- 2) A. G. Riess et al., *Astrophys. J.* **116** (1998), 1009.
- 3) R. A. Knop, et al., *Astrophys. J.* **598** (2003), 102.
- 4) A. G. Riess et al., *Astrophys. J.* **607** (2004), 665.
- 5) D. Sarkar, A. Amblard, D. E. Holz and A. Cooray, arXiv:0710.4143.
- 6) D. E. Holz and E. V. Linder, *Astrophys. J.* **631** (2005), 678.
- 7) K. P. Rauch, *Astrophys. J.* **374** (1991), 83.
- 8) J. Wambsganss, R. Cen, G. Xu and J. P. Ostriker, *Astrophys. J.* **475** (1997), L81.
- 9) A. Cooray, D. Huterer and D. E. Holz, *Phys. Rev. Lett.* **96** (2006), 021301.
- 10) A. J. Barber, *Mon. Not. R. Astron. Soc.* **318** (2000), 195.
- 11) C. Porciani and P. Madau, *Astrophys. J.* **532** (2000), 679.
- 12) P. Valageas, *Astron. Astrophys.* **354** (2000), 767.

- 13) D. E. Holz, *Astrophys. J.* **506** (1998), L1.
- 14) J. A. Frieman, *Comments Astrophys.* **18** (1996), 323.
- 15) H. Martel and P. Premadi, *Astrophys. J.* **673** (2007), 657.
- 16) R. B. Metcalf and J. Silk, *Astrophys. J.* **519** (1999), L1.
- 17) E. Mörtzell, A. Goobar and L. Bergström, *Astrophys. J.* **559** (2001), 53.
- 18) U. Seljak and D. E. Holz, *Astron. Astrophys.* **351** (1999), L10.
- 19) D. E. Holz, *Astrophys. J.* **556** (2001), L71.
- 20) T. Hamana and T. Futamase, *Astrophys. J.* **534** (2000), 29.
- 21) R. B. Metcalf, *Mon. Not. R. Astron. Soc.* **305** (1999), 746.
- 22) E. V. Linder, arXiv:0711.0743.
- 23) J. Jönsson, T. Dahlén, A. Goobar, E. Mörtzell and A. Riess, *J. Cosmol. Astropart. Phys.* **06** (2007), 002.
- 24) B. Ménard and N. Dalal, *Mon. Not. R. Astron. Soc.* **358** (2005), 101.
- 25) Y. Wang, *J. Cosmol. Astropart. Phys.* **03** (2005), 005.
- 26) L. L. R. Williams and J. Song, *Mon. Not. R. Astron. Soc.* **351** (2004), 1387.
- 27) D. E. Holz and R. M. Wald, *Phys. Rev. D* **58** (1998), 063501.
- 28) R. B. Metcalf and J. Silk *Phys. Rev. Lett.* **98** (2007), 071302.
- 29) J. Binney and S. Tremaine, 2008 *Galactic Dynamics, 2nd Edition* (Princeton University Press), p. 751.
- 30) D. Munshi and P. Valageas, astro-ph/0601683.
- 31) M. Sereno, E. Piedipalumbo and M. V. Sazhin, *Mon. Not. R. Astron. Soc.* **335** (2002), 1061.
- 32) M. Goliath and E. Mörtzell, *Phys. Lett. B* **486** (2000), 249.
- 33) Y. Wang, D. E. Holz and D. Munshi, *Astrophys. J.* **572** (2002), L15.
- 34) C. Gunnarsson, *J. Cosmol. Astropart. Phys.* **03** (2004), 002.
- 35) Y. Wang, *Astrophys. J.* **536** (2000), 531.
- 36) Y. Wang and P. Mukherjee, *Astrophys. J.* **606** (2004), 654.
- 37) P. Schneider, J. Elers and E. E. Falco, 1992 *Gravitational Lenses* (New York: Springer, 1992)
- 38) C.-M. Yoo, K. Nakao, H. Kozaki and R. Takahashi, *Astrophys. J.* **655** (2007), 691.
- 39) J. F. Navarro, C. S. Frenk and S. D. M. White, *Astrophys. J.* **490** (1997), 493.
- 40) C. C. Dyer and R. C. Roeder, *Astrophys. J.* **180** (1973), L31.
- 41) R. Kantowski, *Astrophys. J.* **155** (1969), 89.
- 42) B. Jain, U. Seljak and S. White, *Astrophys. J.* **530** (2000), 547.
- 43) J. Wambsganss, R. Cen and J. P. Ostriker, *Astrophys. J.* **494** (1998), 29.
- 44) P. Premadi, H. Martel and R. Matzner, *Astrophys. J.* **493** (1998), 10.

- 45) M. Fukugita, T. Futamase, M. Kasai and E. L. Turner, *Astrophys. J.* **393** (1992), 3.
- 46) H. Asada, *Astrophys. J.* **501** (1998), 473.
- 47) M. Kasai, T. Futamase and F. Takahara, *Phys. Lett. A* **147** (1990), 97.
- 48) K. Watanabe and K. Tomita, *Astrophys. J.* **355** (1990), 1.
- 49) K. Tomita, *Prog. Theor. Phys.* **100** (1998), 79.
- 50) K. Tomita, H. Asada and T. Hamana, *Prog. Theor. Phys. Suppl. No. 133* (1999), 155.
- 51) S. Seitz, P. Schneider and J. Ehlers, *Class. Quantum Grav.* **11** (1994), 2345.
- 52) H. Kozaki, private communication.
- 53) E. L. Turner, J. P. Ostriker and J. R. Gott, III, *Astrophys. J.* **284** (1984), 1.
- 54) M. Vietri and J. P. Ostriker, *Astrophys. J.* **267** (1983), 488.
- 55) L. Bergström, M. Goliath, A. Goobar and E. Mörtzell, *Astron. Astrophys.* **358** (2000), 13.